Dead zones, obstructions, and missed captures: a novel approach for determining the Effective Capture Area for remote camera traps

Carswell, Brendan M.[1*], Avgar, Tal.[2,3], Street, Garrett M.[4], Boyle, Sean P.[1,5] and Eric Vander Wal[1]

1. Department of Biology, Memorial University of Newfoundland and Labrador, Arctic Avenue, St. John's, NL, Canada, A1C 5S7
2. Department of Biology, University of British Columbia, Kelowna, BC, Canada, V1V 1V7
3. Wildlife Science Centre, Biodiversity Pathways Ltd., University of Alberta, Edmonton, AB, Canada, T6G 2E9
4. Department of Wildlife, Fisheries, and Aquaculture, Mississippi State University, Box 9690, Mississippi State, MS 3972, USA
5. School of Science and the Environment, Memorial University of Newfoundland and Labrador Grenfell, University Drive, Corner Brook, NL, Canada, A2H 5G4

*** Corresponding author:** bmcarswell@mun.ca

Data availability: Data and code used in this analysis are available: https://github.com/wildlifeevoeco/EffectiveCaptureArea

Abstract

1. Camera traps have become cemented as an important tool of wildlife research, yet, their utility is now extending beyond researchers, as cameras can contribute to more inclusive methods of place-based wildlife management. From recent advances in analytics and technology, camera trap-based density estimates of wildlife is an emerging field of research. Most camera trap-based density methods require an estimate of the area monitored by each camera, a relatively novel parameter that may be highly variable and is rarely quantified in literature.
2. Here, we developed and tested a standardized field and analytical method allowing us to predict the probability of photographic capture as it varies within the camera viewshed. We investigated how capture probability changes due to environmental influences, i.e., vegetation structure, ambient temperature, speed of subject, time of day, in addition to internal factors from cameras themselves, i.e., sensitivity settings, number of photos taken, and camera trap brand. We then use our method to gain standardized, accurate, and predictable estimates of the area a camera monitors, the Effective Capture Area (ECA).
3. We found that ECAs in our study areas are heavily influenced by location-specific environmental factors, i.e., vegetation structure, technological delays associated with cameras themselves, i.e., refractory period, and custom internal camera settings, i.e., sensitivity, number of photographs taken. We also found that the ECAs computed using our methodology are substantially smaller than reported values in the literature.
4. Imprecision surrounding camera trap viewshed areas can create propagating bias when implementing viewshed-based density estimators. Our method and Effective Capture Area calculation may help increase the reliability of camera trap-based density estimation

methods, provide a framework to help improve camera-trap occupancy modelling, and contribute to more accessible wildlife management practices.

Key Words: Camera trap, motion sensor photography, camera trap viewshed, viewshed density estimator, Effective Capture Area, capture probability

Introduction

In the last five decades, camera traps have become an established method of studying and monitoring wildlife populations (Fisher, 2023; Sollmann, 2018). Camera traps are an easy-to-operate, accessible, relatively affordable, and low-impact method of monitoring wildlife. Camera traps have become an integral part of wildlife management allowing researchers to answer location-based questions of occupancy (e.g., Tobler et al. 2015; Neilson et al. 2018), movement (e.g., Tape and Gustine 2014), and behaviour (e.g., Caravaggi et al. 2017). As a result, camera traps are heavily used among wildlife researchers in general and North American colonial governments in particular. Recently, camera traps are becoming an important tool for Indigenous nations and other interested stakeholders to monitor and manage wildlife on their own lands (Fisher et al., 2021; Kemp, 2023).

Despite their common use, ambiguities around camera trap performance lead to uncertainty and decreasing the quality of inference made from some camera trap-based science. Among their limitations (e.g., Burton et al., 2015; Foster & Harmsen, 2012; Kolowski et al., 2021; Urbanek et al., 2019), empirically estimating the viewshed area a camera trap can monitor is perhaps the least studied, yet, most critical when considering wildlife space use and occupancy. Camera trap data are frequently analyzed using occupancy models or similar frameworks (Burton et al., 2015; MacKenzie et al., 2002, 2017). Such approaches attempt to account for false negatives, i.e., when a species is present in an area but not captured by a

camera, by integrating both the detection probability of a species in a broad study area and the capture probability of a camera photographing a species. Occupancy models can be fit many ways; however, most commonly use *post-hoc* methods such as constructing the detection history of a species across time at each camera trap (MacKenzie et al., 2017). Occupancy models have been shown to be capable of accommodating imperfect detection, i.e., of a species within the broader study area, at camera traps; however, occupancy models are limited in creating a standardized, *apriori* method to assess capture probability, i.e., of an individual in front of a camera trap.

Likelihood-based density and abundance estimates of wildlife species have recently emerged as a novel analysis of camera trap data (e.g., Rowcliffe et al. 2008; Moeller et al. 2018; Nakashima et al. 2020; Becker et al. 2022). Camera trap-based methods, henceforth referred to as viewshed density estimators (Moeller et al., 2023), are a family of statistical models incorporating different processes to estimate wildlife density. For example, Nakashima et al. (2018) developed the Random Encounter Staying Time (REST) model, which measures the amount of time a species spends in front of a camera trap to generate density estimates. Using camera traps to estimate wildlife density promises to lower financial and logistic barriers currently in place for other traditional density estimation methods, e.g., aerial surveys. Some viewshed density estimators do not require the identification of individual animals and thus may constrain less (e.g., no need to mark individuals or census a population) than their traditional counterparts, such as physical mark-recapture methods or aerial flight surveys. Each viewshed density estimator, however, comes with its own set of assumptions and require novel parameters that we lack precision in estimating.

Although viewshed density estimators free us from identifying individual animals, they require a precise estimate of the sampling area that each camera trap monitors (Becker et al., 2022; Moeller et al., 2023; Nakashima et al., 2020; Rowcliffe et al., 2008). Imprecise estimation of the viewshed area is problematic because camera traps, even a large number being used together, monitor a relatively small area—often a minute percentage of a study region. As a result, small errors in the determining the sampling area can lead to large biases in abundance estimates when extrapolating fine-scale density estimates (Moeller et al., 2023). In addition, the theoretical area camera traps monitor often does not align with the realised area. Camera trap manufacturers report an ideal area a camera can monitor given perfect conditions and assuming the camera triggers a photo for every possible activation. For example, Reconyx Hyperfire camera traps, a very popular brand in wildlife research, market a viewshed area extending up to 30 m from the camera trap and 40° angle perpendicular to the camera's lens, an area approximating 315 m^2 (Reconyx 2022; Figure 1A). In reality, environmental factors such as habitat structure, topography, and vegetation (Moeller et al., 2023; Moll et al., 2020; Sultaire et al., 2023), will dictate a cameras viewshed area for each unique location where cameras are placed (Apps and McNutt 2018; Urbanek et al. 2019; Figure 1B).

Researchers also need to account for the probability a photo will be taken given an animal is located within the camera's viewshed, henceforth referred to as capture probability (Findlay et al., 2020; Moeller et al., 2023). Capture probability is more complicated and depends on numerous, likely interacting conditions caused by the physical environment in which cameras are placed, and the internal camera settings. Variation in capture probability is influenced by camera traps Passive Infrared (PIR) motion detectors. PIR motion detectors require recognition of movement within pre-programmed zones, that vary between camera brands and models

(Urbanek et al., 2019), as well as a heat signature that contrast ambient temperature, for a photograph to be taken (Reconyx, 2022; Welbourne et al., 2016). PIR motion detector performance influences capture probability. Yet, how PIR performance contributes to camera monitoring area and thus larger ecological processes remains unknown. Variability in PIR sensor performance may contribute to reports of differential performance throughout the literature, even among similar geography (Apps & McNutt, 2018; Heiniger & Gillespie, 2018).

Internal camera functioning and settings also dictate the viewshed area and how effectively cameras take photos (Apps & McNutt, 2018; Becker et al., 2022; Lepard et al., 2019; Urbanek et al., 2019). For example, even on rapid fire modes, many camera trap user manuals report a 1–2 s refractory period from the time the PIR motion detector is triggered until that photograph can be written to the memory storage device (Del Bosco, 2021; Paula et al., 2014; Reconyx, 2022). Because a camera must reset and register another trigger for subsequent photos to be taken, this phenomenon would be sequential across the entire period an animal is in a camera's viewshed. Thus, the trigger-to-photo delay could create a 'shutter-like' effect where an animal is present in the viewshed but, because of a refractory period, missing in photos for specific locations (Figure 1C). Additionally, to decrease the large number of false triggers, e.g., from vegetation moving, researchers often lower camera trap sensitivity settings, influencing the space a camera trap can monitor. To aid in the identification of species from camera photos, it is common practice to set camera traps to capture multiple rapid-fire photos. As such, researchers often consider a photo series (i.e., all 3, 5, 10 photos) as a single event. As it takes camera traps more time to capture more photographs, however, increasing the number of photos per trigger will reduce the total viewshed area. The effects of internal camera settings have not been

empirically incorporated into camera trap literature, yet, will have compounding influences on how effective camera traps are at photographing wildlife.

Viewshed based density estimators are often criticized for estimates that inconsistently align with traditional density estimation methods (e.g., Palencia et al. 2021; Becker et al. 2022; Fisher et al. 2023; Koetke et al. 2024). Although there may be many explanations for inconsistent results from viewshed density estimators, a lack of accuracy in, or entirely absent incorporation of viewshed area is undoubtedly one reason behind these discrepancies (Moeller et al., 2023). Here, we tested a standardized field protocol to 1) determine the unique bounds of independently placed camera-trap viewsheds (Figure 1B), 2) account for cameras refractory period when sequential photographs are taken (Figure 1C), 3) enumerate a kernel-based photographic capture probability and how it changes with space in front of cameras (Figure 1D), and 4) summarize these capture probability kernels into an *Effective Capture Area*—the scaled area in a cameras viewshed with a 100% capture rate.

Methods

Field methods

To assess capture probability, we tested a standardized field method in two separate case studies. We applied our methods to each camera trap to calculate a novel capture probability metric, unique to each camera trap in our study that in Case Study A) accounts for differences due to habitat and other location specific influences and in Case Study B) incorporates variation resulting from internal camera settings.

Case Study A

We tested 45 camera traps actively deployed as a part of a long-term monitoring program located on Treaty 2 territory, the traditional lands of the Anishinabewaki, Očhéthi Šakówiŋ,

Cree, Oji-Cree, and the Homeland of the Métis peoples (Riding Mountain National Park, Canada; RMNP). Adapting methods from other researchers (Apps & McNutt, 2018; Del Bosco, 2021; Palencia et al., 2021), we established six 20 m long transects, perpendicular to and centred at the camera's optical axis at distances of 3, 5, 10, 12, 15, and 20m (Figure 2) from the lens. These transects were designed to extend past cameras' viewshed to determine the spatial bounds of where the cameras could capture photos. We then performed a 'jog-test' where one researcher attempted to jog at a speed of approximately 2 m/s along each transect, six times, for a total of 36 jogs per camera. With a timer, another researcher initiated each jog-test by triggering the camera using a hand motion to take a photo and recorded the time in seconds it took to jog across the full 20 m. We conducted jog-tests on two different camera brands deployed at our research sites: Reconyx Ultrafire (n = 9; Reconyx, Holmen, USA) and Cuddeback H-1453 (n = 36; Cuddeback, Green Bay, USA). We did not vary any internal settings between trials in Case Study A—all cameras were set to a high sensitivity setting and a single photograph taken for each trigger. Instead, we measured external factors known to affect capture probability. These included: distance from camera trap (McIntyre et al., 2020), vegetation cover in front of cameras (Moeller et al., 2023; Moll et al., 2020), ambient temperature (°C) at time of survey (Urbanek et al., 2019), speed (m/s) of jog for each transect (McIntyre et al., 2020), and camera trap model (Apps and McNutt 2018). In addition, to account for a refractory period after a photographic capture (Del Bosco, 2021; Paula et al., 2014; Reconyx, 2022), we recorded whether cameras captured a photo in the previous two seconds. To measure vegetation cover, we conducted two surveys. (1) a shrub cover survey counting multi-stemmed woody species 10m in front of each camera by usinh the Daubenmire method on a 4 m radius plot (Daubenmire, 1959); and, (2) horizontal cover via a cover pole, placed 10m in front of cameras to quantify vegetation height.

Case Study B

We conducted a series of jog-tests in an open, non-vegetated, flat field in a local park located on traditional unceded territories of the Beothuk and Mi'kma'ki peoples (St. John's, Canada). The trial used a controlled habitat to isolate the effect of internal camera settings on capture probability. In total, we surveyed 27 Reconyx Hyperfire 2 (Reconyx, Holem, USA) camera traps across 3 trials: two during daylight (~1400h) and one after sunset (~2300h). These trials were conducted to measure the influences of the internal camera sensitivity settings (Heiniger & Gillespie, 2018), the number of photos taken per motion trigger and refractory period following a photograph capture (Paula et al., 2014). In addition, we wanted to measure the deterioration of camera trap performance during the nighttime. We held camera settings constant across trials using specific combinations of settings (see Table 1 for all combinations). Due to the lack of visual obstructions during the daytime trials in the open field, we observed a higher-than-expected capture probability on the 20 m transect. Thus, for the two daytime trials we jogged an additional two transects at 30 and 40 m parallel to cameras to fully enumerate the decay of capture probability with distance (Figure 2).

Analytical methods

To calculate a capture rate, we determined the time elapsed (s) between the transect start times and the time when each photograph was taken. Next, we calculated the speed of each transect jog as the time taken to cross each transect divided by transect distance (m/s). We calculated spatial locations where all photographs were taken, i.e., used locations, by multiplying the time elapsed at each photograph by jog velocity to calculate the distance travelled along the transect. For trials where more than one photo were taken per trigger, we filtered photo series down to the first instance when a photograph of the jogger was taken. By using the same jog velocities, and

transect start and end time, we calculated all spatial locations where photographs could have occurred, i.e., available locations. We excluded locations where photographs did occur from the available data thus, creating a 1-m grid-system along each transect where each cell had a binary outcome, whether a photographic capture occurred or not.

Statistical models

We fit the binary capture data using Generalized Additive Mixed Models (GAMMs) using the mgcv package in Program R (Wood 2017) for each case study, separately. We used GAMMs to allow for a non-linear viewshed, that changes with space in front of cameras, by implementing a Gaussian Process spline on the parallel and perpendicular locations from cameras (Wood, 2017). For Case Study A, we created a single, saturated model including covariates measured in the field, i.e., parallel and perpendicular distances from camera trap, percent shrub, and vegetation cover in front of camera, ambient temperature (°C), velocity (m/s) of each jog, camera trap model (categorical), and whether a photograph had occurred in the previous 2 seconds (binary). Additionally, we implemented unique camera trap ID as a random factor smoother (Wood, 2017, 2023). For cameras assessed in Case Study B, in addition to the smoothed parallel and perpendicular locations (McIntyre et al., 2020), we included categorical covariates for each of the variables of interest: camera sensitivity setting, number of photos taken per motion trigger, time of day, and whether a capture had been taken in the previous two seconds (Table 2).

We used both GAMM models, along with covariate data from each trial, and the *predict_gamm()* function (Wood 2023) to predict the probability of photographic capture occurring across a 1x1-m extrapolated spatial grid both between transect lines and beyond the cameras' field of view, 10 m in both directions of the focal axis 40 m from the lens (e.g., Figure 1D). We further applied these models to also predict capture probability at any cameras where

data were collected (e.g., vegetation cover, ambient temperature etc.) but that were not included in the trial tests.

Our primary goal was to determine the area that camera traps monitor with 100% capture probability: the Effective Capture Area (ECA). To estimate ECA, we multiplied the average probability of photographic capture in each of 800 predicted grid cells by their area ($1m^2$). Our approach assumes equivalency between predicted probabilities of photographic capture and the percent area monitored in each cell. Though this assumption of equivalency may have varying validity depending on the study, we think here our assumption is robust as we rely heavily on the average effect of covariates (as discussed below). Additionally, our study design, which assesses locations multiple times in quick succession, has been shown to reduce bias in similar space-for-time equivalencies (Kendall and White, 2009). Thus, the resulting values represent the equivalent area within each cell that a photograph would be captured with certainty. For example, a capture probability of 0.33 in a 1 m^2 cell is equivalent to having 0.33 m^2 of area where a capture will occur 100% of the time. We then took the sum of predicted values across all cells, representing the adjusted space in front of cameras with a 100% capture probability (Figure 1E), which we defined as the ECA. In addition, we determined standard error and confidence bounds for all ECA calculation. Because the ECA was determined through prediction, we wanted to ensure sufficient predictive accuracy of our analysis for our Case Study A field trial. Because a camera's monitoring area is unknown, we employed *k*-folds cross validation on the probability of photographic capture for spatial locations in front of each camera (Geisser, 1975). Using unique camera ID as a blocking variable, we withheld entire cameras to assess the predictive accuracy of each 1x1-m cell across camera traps and thus the validity of our method at

cameras where jog-tests were not conducted (Fielding & Bell, 1997). We generated Receiver Operating Characteristics (ROC) Area Under Curve (AUC) scores for each of these validations.

To determine how strongly the numeric covariates in Case Study A influence a cameras ECA, we calculated a *post-hoc* effect size through prediction. We ran separate predictions for each numeric covariate of interest—percent shrub cover, percent horizontal cover, velocity of jog, and ambient temperature—and generated ECA values across the observed range of each covariate while holding all other variables at their mean values. For example, horizontal cover ranged from 42–99%, thus we ran an ECA prediction for each unit (percent) value in that range. Next, we calculated the mean of all unit-change differences in ECA predictions. The resulting values represent the mean influence of a 1-unit change by a covariate on a camera's ECA. For Case Study B, we ran similar predictions, but for each level in the categories of interest, i.e., sensitivity setting and number of photos per trigger, while holding all other variables at constant values.

Results

Case Study A

We determined the predicted probability of a successful photographic capture occurring within a camera viewshed at a 1x1-m resolution (Figure 3A). For all cameras where we collected local site data, we calculated their unique capture probability distributions and scaled them to an ECA. For example, Figure 3A represents a Reconyx Ultrafire camera within our Riding Mountain National Park field site, with an average 62 % shrub cover, 79% horizontal cover, and an ambient air temperature of 1.5°C during survey time. Assuming a subject moving at a velocity of 2 m/s in the cameras viewshed area, we scaled these probabilities to an ECA of 15 m^2 and a standard error ranging from 8–27 m^2 (Figure 3A). Ambient temperature at time of jog-test

surveys ranged from -2–10°C, velocity of each jog from 0.76–2.86 m/s, percent shrub cover from 0–176 %, and percent horizontal cover from 42–98 %.

Covariates in the model showed varying levels of significance (Table 2). The parallel and perpendicular locations from camera traps, fit in a Gaussian process spline, was highly significant ($F = 42.655$, $p < 0.001$). In addition, the binary refractory period variable showed a significant negative relationship with photographic capture ($\beta = -0.955$, $p < 0.001$). Other covariates showed varying effects on ECAs (see Table 2). Percent unit changes in shrub ($\bar{x} = 0.211 m^2$) and horizontal cover ($\bar{x} = 0.213\ m^2$) had a relatively small influence on ECA. Absolute differences between the largest and smallest ECA prediction, however, were larger. The difference between the largest and smallest ECA was 86 m^2 for shrub cover and 50 m^2 for horizontal cover (Figure 6). A unit change in temperature (°C) had a larger influence on ECA, with a mean of $2.546 m^2$, and a maximum of $79 m^2$ difference between the maximum and minimum ECA predictions (Figure 6). Finally, unit changes in velocity (m/s) of each jog had the largest influence of ECA prediction, with a mean of $34.630 m^2$ and a maximum of $69 m^2$ between the largest and smallest predictions (Figure 6). The predictive accuracy of the model, assessed at each 1x1 m cell between camera traps, was good (AUC=0.76; Boyce et al. 2002).

Case Study B

Our controlled, open field trials suggested that predetermined sensitivity settings have a large, significant influence on the probability of photographic capture and thus the ECA (Table 2). For example, our model estimated a maximum difference of approximately 250 m^2 in ECAs between the lowest and highest sensitivity settings on the Reconyx Hyperfire 2 cameras (Figure 4). The number of photos taken per trigger had a significant negative influence on ECA, where 3 and 5 photographs per capture produced significantly lower ECAs than 1 photo but were not different

from eachother (Table 2, Figure 4). Jog-tests conducted in the daytime produced significantly higher ECAs ($\bar{x}$ = 151 m^2, SE =122–191 m^2) than the post-sunset jog-tests ($\bar{x}$ = 73 m^2, SE = 51–101 m^2, Table 2, Figure 5). The smoothed terms of the Case Study B model, i.e., parallel and perpendicular locations fit in a Gaussian process spline (F = 39.969, p <0.001), and refractory period variable (β = 1.669, p <0.001) were both highly significant.

Discussion

Our study provides a tested field and analytical framework for determining the Effective Capture Area (ECA) of camera traps, an accurate viewshed area with a 100% capture probability, that incorporates capture probability and how it is influenced by local environmental variables and internal camera settings. We determined the ECA through a spatially predictive kernel-based photographic capture probability analysis, providing new insight into how capture probability varies within a camera's viewshed. Our analysis suggested that capture probabilities and the associated ECA are sensitive metrics and can vary substantially depending on both environmental influences and user-defined settings. Understanding and accurately estimating the ECA is crucial when implementing viewshed density estimators and may also contribute how researchers interpret camera-based occupancy analyses.

Case Study A

ECA values generated from our Case Study A model are substantially smaller than other published literature. For example, an average Reconyx Ultrafire camera in our study was estimated to monitor an area of 16m^2 (ranging from 12–22m^2) with a perfect capture probability. Our average Reconyx ECA, in the Case Study A field trial, was less than 10% of the total possible area the camera trap advertises (Reconyx, 2022) and still smaller than other published monitoring areas (Becker et al., 2022; Garland et al., 2020). Thus, if implementing the previous

detection areas, i.e., 16m^2 vs 315m^2, on viewshed density estimators, density estimates would differ by an entire order of magnitude. Although cameras' capture probability area cannot be unilaterally applied across different studies in varying geography and with different external influences, our work highlights the importance of conducting a standardized test on all cameras of a study when attempting to estimate monitoring areas.

In Case Study A, our goal was to develop an accurate metric to estimate the physical space camera traps monitor, specifically for use with viewshed density estimators. Though not statistically significant, our environmental covariates, i.e., shrub cover, horizontal cover, temperature, and jog velocity, still contributed considerable variability in ECA. For example, when holding other covariates at mean values, average per-unit changes in vegetation structure, shrub cover and horizontal cover can influence ECA by ~0.2 m^2. Although changes are small over single percentage changes, if we consider cameras with 50% differences in either shrub or horizontal cover, ECA could be influenced by over 10 m^2. Vegetation influences are likely even greater in affecting ECA, considering shrub and horizontal cover are additive, resulting in a compounded effect on ECA.

We detected a relatively small influence of unit changes of temperature on ECA, with a mean of ~2 m^2 per °C. The small influence of temperature is intuitive given the short duration when we conducted jog-tests. For example, we conducted our Case Study A jog-tests on the edges of winter (April and November 2023). The time of year allowed us to safely access remote field sites, in addition to providing conditions consistent with when traditional density estimation surveys take place (e.g., aerial flight surveys in late winter) for future applications of our work. As a result, many of our covariates show little range. Ambient air temperatures at time of survey only ranged from -2–10°C, and total shrub was measured after leaf senescence in the fall,

limiting observed variability. Although we would not expect camera traps to decrease performance until -20°C or below (Reconyx, 2022), it is worth noting that other research has observed camera traps performing best around 0°C, where higher false-negatives occur in positive temperature ranges (Jacobs & Ausband, 2018), and negative temperature ranges and associated weather can contribute to decreased performance (Maile et al., 2023). Conducting jog-tests during other seasons and within a greater range of forest types and habitat will likely contribute to detecting statistical differences in environmental covariates and help determine if a cameras ECA varies more substantially across space and time (e.g., as in McIntyre et al., 2020; Moeller et al., 2023; Moll et al., 2020; Sultaire et al., 2023; Urbanek et al., 2019).

Though our jog-tests were conducted at relatively consistent velocities, we detected a large difference in ECA between unit (m/s) changes in jog velocity, with a mean of ~35 m^2. Further, our predictions show that slower jog speeds lead to higher ECAs. Our jog velocity results stand in contrast to previous findings (e.g., Del Bosco, 2021) who found that faster jog velocities generally lead to higher capture rates at camera traps. This velocity discrepancy may be explained by the habitat in which jog-tests were conducted. Specifically, our tests took place in primary and secondary conifer and mixed forests where as Del Bosco's (2021) work occurred in more open, sagebrush-mountain habitat. We suggest researchers consider both habitat composition as well as effective movement speed of the species of interest when implementing the jog-test method.

Cross-validation of the probability of photographic capture occurring in each 1x1-m cell assessed during jog-tests highlighted that our ECA modelling framework has useful predictive accuracy. In addition, environmental covariates explained substantial variation in our model, as determined through average unit-changes. The variation explained by covariates, along with our

cross-validation results, suggest that, in our geography, we can predict ECA well at cameras where we did not conduct jog-tests, but did collect vegetation data.

Case Study B

Overall, sensitivity settings on Reconyx Hyperfire II cameras greatly influenced the predicted ECA. Differences between lower sensitivity settings were smaller but became more pronounced as the sensitivity settings became higher. These results show how drastically a camera traps monitoring zone can change with sensitivity settings, e.g., from ~75m^2 to ~350m^2 in open conditions, reinforcing the importance of consistency and assessing cameras in each location they are placed. Our results highlight the balance researchers need to consider when altering sensitivity settings to decrease false negative photographic captures, while risking tremendous loss of area in photographable space.

Predicted ECAs for trials set to take 3 or 5 photos per trigger were significantly smaller than trials with 1 photo per trigger, but not different from each other. As we take more photographs per event, the camera trap will be less able to capture future photographs. This is simply because, even on rapid fire modes, it takes longer for to capture and write 3 or 5 photographs than a single photograph. When considering a refractory period as well (discussed below) setting cameras to take more photos will greatly reduce the available time a camera has to take a photo and thus, the ECA. Though additional photos per trigger can be very useful in the identification of species, additional photos have an overall negative influence on a cameras viewshed area. Intuitively, trials conducted in the daytime had significantly higher ECAs compared to post-sunset trials. A lower nighttime ECA is likely because the visible range of the camera trap will be reduced during nighttime, in addition to a reduced contrast from the subject

to the background. Nighttime ECAs will be particularly important on camera trap studies for species that are predominately nocturnal, as viewshed area may be lower than anticipated.

Camera refractory period

Our two case studies observed opposite effects of the refractory period variable. In Case Study A, we observed a significant negative relationship between capture probability within a 1x1-m cell and whether a photo was captured in the previous two seconds. The refractory period result met our null expectations that, due to delay, our cameras deployed in the field were less able to capture photos immediately after a previous photo had been taken. Our Case Study B model, however, exhibited the opposite trend and the refractory period variable/ was significantly positively correlated with capture probability, i.e., photos were more likely to be taken immediately following a previous capture. These contrasting results were likely due to the way we structured the Case Study B trials, where many trials took more than one photo per trigger. For example, in trials where cameras took 3 or 5 images per trigger, by artifact of camera trap shutter speed, the time it takes to capture 3 or 5 images is longer than 1 image. Thus, the refractory period of a camera would be longer if the camera trap is set to capture more images per trigger, e.g., potentially 3–6 seconds after the first photo in the series is captured.

The elongated refractory period caused by trials with more than 1 photograph taken per trigger is also likely responsible for the divergence in capture probability observed in our graphical representation of ECA in Case Study B (Figure 5). During trials where cameras were set to take multiple photos, if captures were registered at the start and end of transects, where a refractory period occurred near the midpoint of the trial, the pattern we observe of decreased capture probability directly perpendicular to cameras past ~14m could be explained (Figure 5). The gap in photograph captures would not be observed at closer distances to cameras because of

camera lens angle—there is physically less space within a camera's viewshed, explaining the gap in detection probability for trials with multiple photos per activation (Figure 5).

Limitations and future directions

The functioning and performance of camera traps remains a heavily understudied facet of the field that certainly influences occupancy and density-based camera analyses and thus interpretation of camera trap-based research. In our work, how PIR sensors perform across temperature and seasonal gradients is particularly important. PIR detectors in camera traps function by sensing a difference in temperature of a subject from ambient temperature, in addition to movement, to capture a photograph (Reconyx, 2022; Welbourne et al., 2016). The interacting effects of ambient temperature and seasonality will influence the amount of heat wildlife subjects will emit. For example, in winter, ungulates have thick winter coats that allow them to retain heat and survive harsh conditions and as such, less heat may be escaping the coat (Parker and Robbins 2018). A lack of heat emission has been previously observed in thermal imaging studies, where thermal cameras have a difficult time picking up certain species during certain temperature ranges (Kuhn & Meyer, 2009; Zabel et al., 2023). As a result, capture probability may be even lower during mid-winter months for some wildlife species.

Camera traps are influenced, to some degree, by the size of the subject they are capturing (DeWitt & Cocksedge, 2023). For example, Urbanek et al. (2019) observed that raw number of photographs at camera traps were similar for species groups that were generally the same size. The pattern in Urbanek et al. (2019) data suggests a potential trigger threshold where above certain body sizes, the number of photographs taken (and thus ECA) may increase. We think that our approach will work well for some species, particularly ungulates, based on height, but would not work well for others, such as species generally smaller than humans.

Our GAMM model was developed to incorporate important predictor variables specifically at our field site in Riding Mountain National Park (MB, Canada). We hypothesized the largest influencing factor to cameras would be vegetation, specifically shrub cover. Although vegetation cover in our study had a relatively lower influence on ECA (Table 2, Figure 6), the importance of different predictor variables, will likely depend on the geography and habitat conditions of the study. For example, topography (Sultaire et al., 2023) and weather (Madsen et al., 2020) have been found to influence camera trap capture probabilities in some geographies. Thus, if implementing our method, researchers should consider all potential important predictor variables that may influence capture probability at their study sites.

Conclusion

We use a standardized, *apriori* field and analytical protocol to predict the variable probability of photographic capture at camera traps while incorporating internal and environmental influences on camera performance. We use our predictions of capture probability to estimate the Effective Capture Area (ECA), a novel estimator that represents the scaled area in front of cameras with a 100% capture probability. Our results highlight how variable camera trap performance can be and provide a framework for researchers and other camera trap users to account for variable viewshed areas and capture probabilities for some taxa of wildlife. ECA may contribute to increasing the reliability and precision of camera-based occupancy modelling as well as viewshed density estimators and thus forward the growing branch of camera trap research.

Literature cited

Apps, P., & McNutt, J. W. (2018). Are camera traps fit for purpose? A rigorous, reproducible and realistic test of camera trap performance. *African Journal of Ecology*, *56*(4), 710–720. https://doi.org/10.1111/aje.12573

Becker, M., Huggard, D. J., Dickie, M., Warbington, C., Schieck, J., Herdman, E., Serrouya, R., & Boutin, S. (2022). Applying and testing a novel method to estimate animal density from motion-triggered cameras. *Ecosphere*, *13*(4). https://doi.org/10.1002/ecs2.4005

Boyce, M. S., Vernier, P. R., Nielsen, S. E., & Schmiegelow, F. K. A. (2002). Evaluating resource selection functions. *Ecological Modelling*, *157*, 281–300. https://doi.org/10.1016/S0304-3800(02)00200-4

Burton, A. C., Neilson, E., Moreira, D., Ladle, A., Steenweg, R., Fisher, J. T., Bayne, E., & Boutin, S. (2015). Wildlife camera trapping: A review and recommendations for linking surveys to ecological processes. *Journal of Applied Ecology*, *52*(3), 675–685. https://doi.org/10.1111/1365-2664.12432

Caravaggi, A., Banks, P. B., Burton, A. C., Finlay, C. M. V., Haswell, P. M., Hayward, M. W., Rowcliffe, M. J., & Wood, M. D. (2017). A review of camera trapping for conservation behaviour research. *Remote Sensing in Ecology and Conservation*, *3*(3), 109–122. https://doi.org/10.1002/rse2.48

Daubenmire, R. (1959). A canopy-coverage method of vegetational analysis. *Northwest Science*, *33*, 43–64.

Del Bosco, T. (2021). *An eulerian perspective on spring migration in mule deer* [MSc. thesis]. Utah State University.

DeWitt, P. D., & Cocksedge, A. G. (2023). A simple framework for maximizing camera trap detections using experimental trials. *Environmental Monitoring and Assessment*, *195*(11), 1381. https://doi.org/10.1007/s10661-023-11945-9

Fielding, A. H., & Bell, J. F. (1997). A review of methods for the assessment of prediction errors in conservation presence/absence models. *Environmental Conservation*, *24*(1), 38–49. https://doi.org/10.1017/S0376892997000088

Findlay, M. A., Briers, R. A., & White, P. J. C. (2020). Component processes of detection probability in camera-trap studies: Understanding the occurrence of false-negatives. *Mammal Research*, *65*(2), 167–180. https://doi.org/10.1007/s13364-020-00478-y

Fisher, J. T. (2023). Camera trapping in ecology: A new section for wildlife research. *Ecology and Evolution*, *13*(3), e9925. https://doi.org/10.1002/ece3.9925

Fisher, J. T., Dickie, M., Burgar, J. M., Burton, A. C., & Serrouya, R. (2023). Density estimates of unmarked mammals: comparing two models and assumptions across multiple species and years. *Canadian Journal of Zoology*, *102(3)*, 286–297. cjz-2023-0055. doi:10.1139/cjz-2023-0055.

Fisher, J. T., Grey, F., Anderson, N., Sawan, J., Anderson, N., Chai, S.-L., Nolan, L., Underwood, A., Amerongen Maddison, J., Fuller, H. W., & Frey, S. (2021). Indigenous-led camera-trap research on traditional territories informs conservation decisions for resource extraction. *FACETS*, *6*, 1266–1284. https://doi.org/10.1139/facets-2020-0087

Foster, R. J., & Harmsen, B. J. (2012). A critique of density estimation from camera-trap data. *The Journal of Wildlife Management*, *76*(2), 224–236. https://doi.org/10.1002/jwmg.275

Garland, L., Neilson, E., Avgar, T., Bayne, E., & Boutin, S. (2020). Random Encounter and Staying Time Model Testing with Human Volunteers. *The Journal of Wildlife Management*, *84*(6), 1179–1184. https://doi.org/10.1002/jwmg.21879

Geisser, S. (1975). The predictive sample reuse method with applications. *Journal of American Statistical Association*, *70*, 320–328. https://doi.org/10.1080/01621459.1975.10479865

Heiniger, J., & Gillespie, G. (2018). High variation in camera trap-model sensitivity for surveying mammal species in northern Australia. *Wildlife Research*, *45*(7), 578. https://doi.org/10.1071/WR18078

Jacobs, C. E., & Ausband, D. E. (2018). An evaluation of camera trap performance – What are we missing and does deployment height matter? *Remote Sensing in Ecology and Conservation*, *4*(4), 352–360. https://doi.org/10.1002/rse2.81

Kemp, C. (2023). *Optimizing Community-Based Wildlife Monitoring: Prioritizing Indigenous Knowledge and Values* [MSc. thesis]. University of Guelph.

Kendall, W. L., & White, G. C. (2009). A cautionary note on substituting spatial subunits for repeated temporal sampling in studies of site occupancy. *Journal of Applied Ecology, 46*, 1182–1188. https://doi.org/10.1111/j.1365-2664.2009.01732.x

Koetke, L. J., Hodder, D. P., & Johnson, C. J. (2024). Using camera traps and N-mixture models to estimate population abundance: Model selection really matters. *Methods in Ecology and Evolution, 2024;00:1–16.* https://doi.org/10.1111/2041-210X.14320

Kolowski, J. M., Oley, J., & McShea, W. J. (2021). High-density camera trap grid reveals lack of consistency in detection and capture rates across space and time. *Ecosphere*, *12*(2). https://doi.org/10.1002/ecs2.3350

Kuhn, R., & Meyer, W. (2009). Infrared thermography of the body surface in the Eurasian otter Lutra lutra and the giant otter Pteronura brasiliensis. *Aquatic Biology*, *6*, 143–152. https://doi.org/10.3354/ab00176

Lepard, C. C., Moll, R. J., Cepek, J. D., Lorch, P. D., Dennis, P. M., Robison, T., & Montgomery, R. A. (2019). The influence of the delay-period setting on camera-trap data storage, wildlife detections and occupancy models. *Wildlife Research*, *46*(1), 37. https://doi.org/10.1071/WR17181

MacKenzie, D. I., Nichols, J. D., Lachman, G. B., Droege, S., Andrew Royle, J., & Langtimm, C. A. (2002). Estimating site occupancy rates when detection probabilities are less than one. *Ecology*, *83*(8), 2248–2255. https://doi.org/10.1890/0012-9658(2002)083[2248:ESORWD]2.0.CO;2

MacKenzie, D. I., Nichols, J. D., Royle, J. A., Pollock, K. H., Bailey, L. L., & Hines, J. E. (2017). *Occupancy estimation and modelling: Inferring patterns and dynamics of species occurence.* Elsevier.

Madsen, A. E., Corral, L., & Fontaine, J. J. (2020). Weather and exposure period affect coyote detection at camera traps. *Wildlife Society Bulletin*, *44*(2), 342–350. https://doi.org/10.1002/wsb.1080

Maile, R. E., Duggan, M. T., & Mousseau, T. A. (2023). The successes and pitfalls: Deep-learning effectiveness in a Chernobyl field camera trap application. *Ecology and Evolution*, *13*(9), e10454. https://doi.org/10.1002/ece3.10454

McIntyre, T., Majelantle, T. L., Slip, D. J., & Harcourt, R. G. (2020). Quantifying imperfect camera-trap detection probabilities: Implications for density modelling. *Wildlife Research*, *47*(2), 177. https://doi.org/10.1071/WR19040

Moeller, A. K., Lukacs, P. M., & Horne, J. S. (2018). Three novel methods to estimate abundance of unmarked animals using remote cameras. *Ecosphere*, *9*(8), e02331. https://doi.org/10.1002/ecs2.2331

Moeller, A. K., Waller, S. J., DeCesare, N. J., Chitwood, M. C., & Lukacs, P. M. (2023). Best practices to account for capture probability and viewable area in camera-based abundance estimation. *Remote Sensing in Ecology and Conservation*, *9*(1), 152–164. https://doi.org/10.1002/rse2.300

Moll, R. J., Ortiz-Calo, W., Cepek, J. D., Lorch, P. D., Dennis, P. M., Robison, T., & Montgomery, R. A. (2020). The effect of camera-trap viewshed obstruction on wildlife detection: Implications for inference. *Wildlife Research*, *47*(2), 158. https://doi.org/10.1071/WR19004

Nakashima, Y., Fukasawa, K., & Samejima, H. (2018). Estimating animal density without individual recognition using information derivable exclusively from camera traps. *Journal of Applied Ecology*, *55*(2), 735–744. https://doi.org/10.1111/1365-2664.13059

Nakashima, Y., Hongo, S., & Akomo-Okoue, E. F. (2020). Landscape-scale estimation of forest ungulate density and biomass using camera traps: Applying the REST model. *Biological Conservation*, *241*, 108381. https://doi.org/10.1016/j.biocon.2019.108381

Neilson, E. W., Avgar, T., Burton, A. C., Broadley, K., & Boutin, S. (2018). Animal movement affects interpretation of occupancy models from camera-trap surveys of unmarked animals. *Ecosphere*, *9*(1). https://doi.org/10.1002/ecs2.2092

Palencia, P., Rowcliffe, J. M., Vicente, J., & Acevedo, P. (2021). Assessing the camera trap methodologies used to estimate density of unmarked populations. *Journal of Applied Ecology*, *58*(8), 1583–1592. https://doi.org/10.1111/1365-2664.13913

Parker, K. L., & Robbins, C. T. (2018). Thermoregulation in ungulates. In *Bioenergetics of wild herbivores* (pp. 161–182). CRC press.

Paula, J. J. S., Bispo, R. M. B., Leite, A. H., Pereira, P. G. S., Costa, H. M. R. G., Fonseca, C. M. M. S., Mascarenhas, M. R. T., & Bernardino, J. L. V. (2014). Camera-trapping as a methodology to assess the persistence of wildlife carcasses resulting from collisions with human-made structures. *Wildlife Research*, *41*(8), 717. https://doi.org/10.1071/WR14063

Reconyx. (2022). *Reconyx Hyperfire 2 high performance camera instruction manual*. https://www.reconyx.com/img/file/HyperFire_2_User_Guide_2018_07_05_v5.pdf

Rowcliffe, J. M., Field, J., Turvey, S. T., & Carbone, C. (2008). Estimating animal density using camera traps without the need for individual recognition. *Journal of Applied Ecology*, *45*(4), 1228–1236. https://doi.org/10.1111/j.1365-2664.2008.01473.x

Sollmann, R. (2018). A gentle introduction to camera-trap data analysis. *African Journal of Ecology*, *56*(4), 740–749. https://doi.org/10.1111/aje.12557

Sultaire, S. M., Millspaugh, J. J., Jackson, P. J., & Montgomery, R. A. (2023). The influence of fine-scale topography on detection of a mammal assemblage at camera traps in a mountainous landscape. *Wildlife Biology*, *2023*(2). https://doi.org/10.1002/wlb3.01026

Tape, K. D., & Gustine, D. D. (2014). Capturing Migration Phenology of Terrestrial Wildlife Using Camera Traps. *BioScience*, *64*(2), 117–124. https://doi.org/10.1093/biosci/bit018

Tobler, M. W., Zúñiga Hartley, A., Carrillo-Percastegui, S. E., & Powell, G. V. N. (2015). Spatiotemporal hierarchical modelling of species richness and occupancy using camera trap data. *Journal of Applied Ecology*, *52*(2), 413–421. https://doi.org/10.1111/1365-2664.12399

Urbanek, R. E., Ferreira, H. J., Olfenbuttel, C., Dukes, C. G., & Albers, G. (2019). See what you've been missing: An assessment of Reconyx® PC900 Hyperfire cameras. *Wildlife Society Bulletin*, *43*(4), 630–638. https://doi.org/10.1002/wsb.1015

Welbourne, D. J., Claridge, A. W., Paull, D. J., & Lambert, A. (2016). How do passive infrared triggered camera traps operate and why does it matter? Breaking down common misconceptions. *Remote Sensing in Ecology and Conservation*, *2*(2), 77–83. https://doi.org/10.1002/rse2.20

Wood, S. (2017). *Generalized Additive Mixed Models: An introduction with R*. CRC press.

Wood, S. (2023). mgcv: Mixed GAM computation vehicle with automatic smoothness estimation. *R Package: Version 1.9-0*. https://cran.r-project.org/web/packages/mgcv/index.html

Zabel, F., Findlay, M. A., & White, P. J. C. (2023). Assessment of the accuracy of counting large ungulate species (red deer *Cervus elaphus*) with UAV-mounted thermal infrared cameras during night flights. *Wildlife Biology*, *2023*(3), e01071. https://doi.org/10.1002/wlb3.01071

Table 1. The combinations of camera sensitivity settings, number of photos taken for each passive infrared motion trigger, and time of day we implemented on to Reconyx Hyperfire 2 (*n* = 26) camera traps during Case Study B, in a controlled, open field setting, in St. John's Canada.

Trial type	Number of cameras	Sensitivity setting	Number of photos per trigger	Time of day
Sensitivity	3	Low	1	Day
	3	Medium	1	Day
	3	Very high	1	Day
Number of photos	3	High	1	Day
	3	High	3	Day
	3	High	5	Day
Night	9	High	1	Night

Table 2. Binary Generalized Additive Mixed Models (GAMMs) used in determining the Effective Capture Areas of (a) camera traps (n = 46) in Riding Mountain National Park, Canada and (b) camera traps (n = 27) in a non-vegetated local park near St. John's, Canada. Showing different predictor variables used in each model, with their respective explanations, coefficient values, and probability values. Both models contain the parallel and perpendicular locations in front of each camera trap with splines implemented, in addition to unique camera identification implemented as a random intercept.

Riding Mountain National Park field data (Case Study A) model:				Controlled setting data (Case Study B) model:			
Covariate	Explanation	Coefficient (χ^2 for smoothed terms)	p-value	Covariate	Explanation	Coefficient (χ^2 for smoothed terms)	p-value
s(parallel distance, perpendicular distance)	Gaussian process spline of the parallel (locations in front) and perpendicular (locations to the side) of camera traps	**829.978**	**<0.001**	**s(parallel distance, perpendicular distance)**	Gaussian process spline on parallel (in front) and perpendicular locations (to the side) of camera traps	**1009.3**	**<0.001**
te(shrub cover, horizontal cover)	Tensor product spline of percent shrub cover (determined by Daubenmire plots) and horizontal cover (determined from cover pole)	1.435	0.707	Low camera sensitivity	Categorical variable for the sensitivity setting chosen on each camera trap for a specific trial	Set as intercept	
				Medium camera sensitivity		**1.076**	**<0.001**
				High camera sensitivity		**1.837**	**<0.001**
				Very high camera sensitivity		**3.479**	**<0.001**
Photo taken in previous 2 seconds	Binary variable of whether the camera took a photo in the previous two seconds	**-1.064**	**<0.001**	1 photo per trigger	Categorical variable for the number of photos taken per trigger setting chosen on each camera trap for a specific trial	Set as intercept	
				3 photos per trigger		**-1.266**	**<0.001**
				5 photos per trigger		**-1.186**	**<0.001**
Jog velocity	Velocity of each transect jog during the field surveys	0.211	0.126	Nighttime trial	Whether or not trials occurred during daylight or night hours	Set as intercept	
				Day-time trial		**1.072**	**<0.001**
Ambient temperature	Ambient temperature (°C) measured from camera traps at time of survey	0.082	0.428	**Photo taken in previous 2 seconds**	Binary variable of whether the camera took a photo in the previous two seconds	**0.173**	**0.047**
Camera model	Categorical variable for the brand of camera	-0.370	0.527				

	trap (Reconyx or cuddeback) used in the field trials						
s**(unique camera ID)**	Random factor smooth implemented on each unique camera trap	**358.793**	**<0.001**	**s(unique camera ID)**	Random factor smooth implemented on each unique camera trap	**24.7**	**<0.001**

611

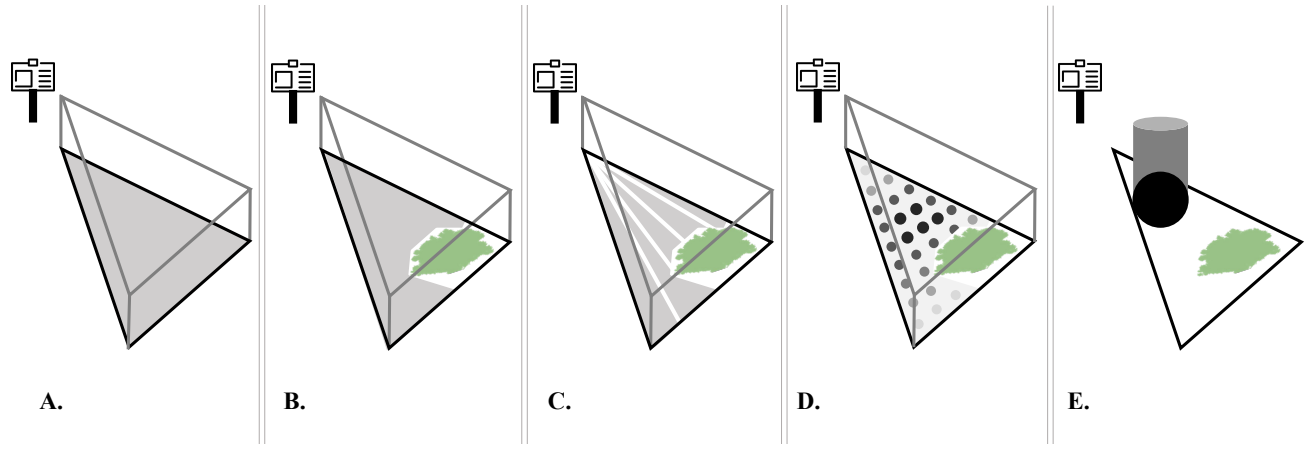

Figure 1. Viewshed areas for camera traps (grey shading) **A.** theoretical viewshed based on Reconyx Hyperfire 2 specification, e.g., 40° angle and 30 m distance, **B.** theoretical viewshed that might account for vegetation obstruction **C.** a theoretical viewshed that addresses refractory period in a camera trap, e.g., a camera could be triggered in the entire viewshed, but lacking photos for certain locations **D.** differential capture probabilities in a viewshed, where darker dots indicate a higher probability of photographic capture occurring and **E.** differential capture probabilities scaled down into our *Effective Capture Area*—an estimated area in front of a camera with 100% capture probability.

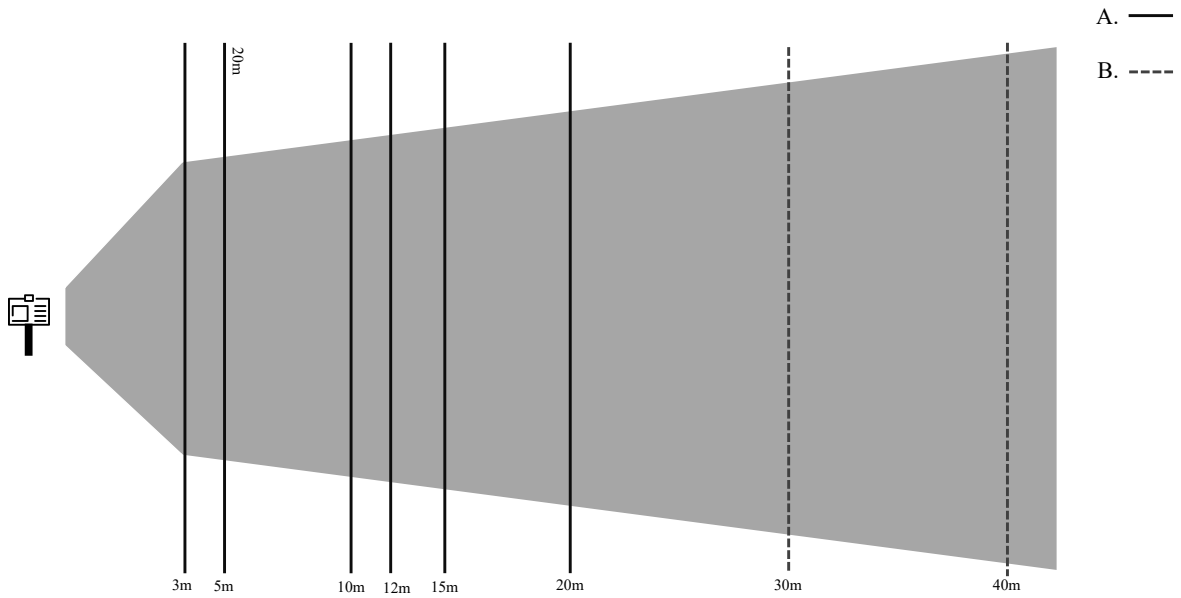

Figure 2. Transects and distances assessed on 'jog-tests' during **A.** field trials in Riding Mountain National Park, Canada (*n* = 45 cameras) at 3, 5, 10, 12, 15, and 20 m perpendicular to each camera trap and **B.** additional transects assessed at our daytime controlled setting trials in St. John's, Canada (*n* = 26 cameras) at 3, 5, 10, 12, 15, 20, 30, and 40 m perpendicular to camera traps. All transects were assessed 6 times at an approximate velocity of 2 m/s.

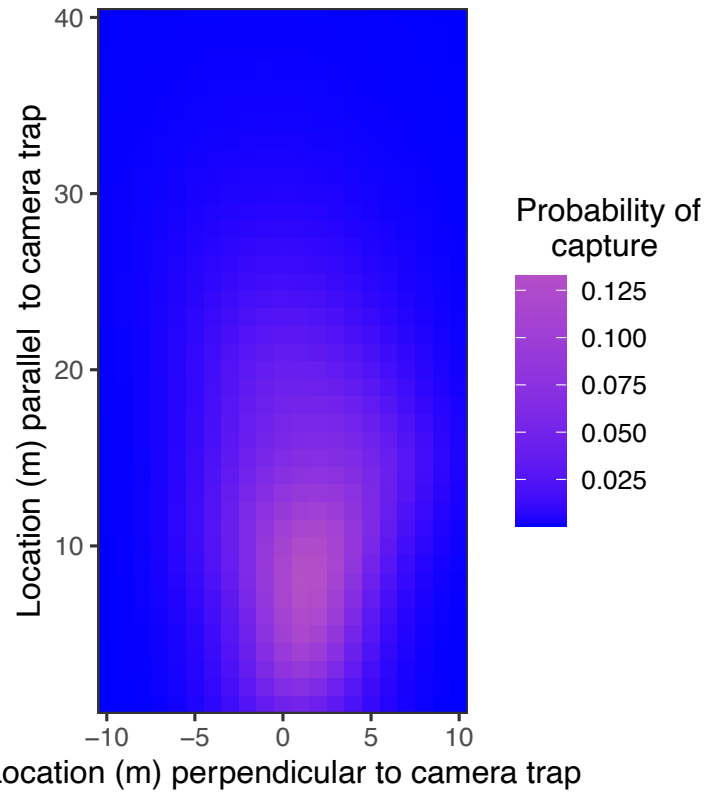

Figure 3. Predicted probabilities of photographic capture, determined by Generalized Additive Mixed Models, on a 1x1 m grid for an average Reconyx Ultrafire camera in Case Study A, with 62 % shrub cover, a subject moving at a 2 m/s velocity, and an ambient air temperature of 1.5°C. The predicted Effective Capture Area (± 1 SE) for this camera was determined to be 15 m^2 (8–27m^2). The camera traps is located at position [0,0] on the grid.

Effective Capture Area

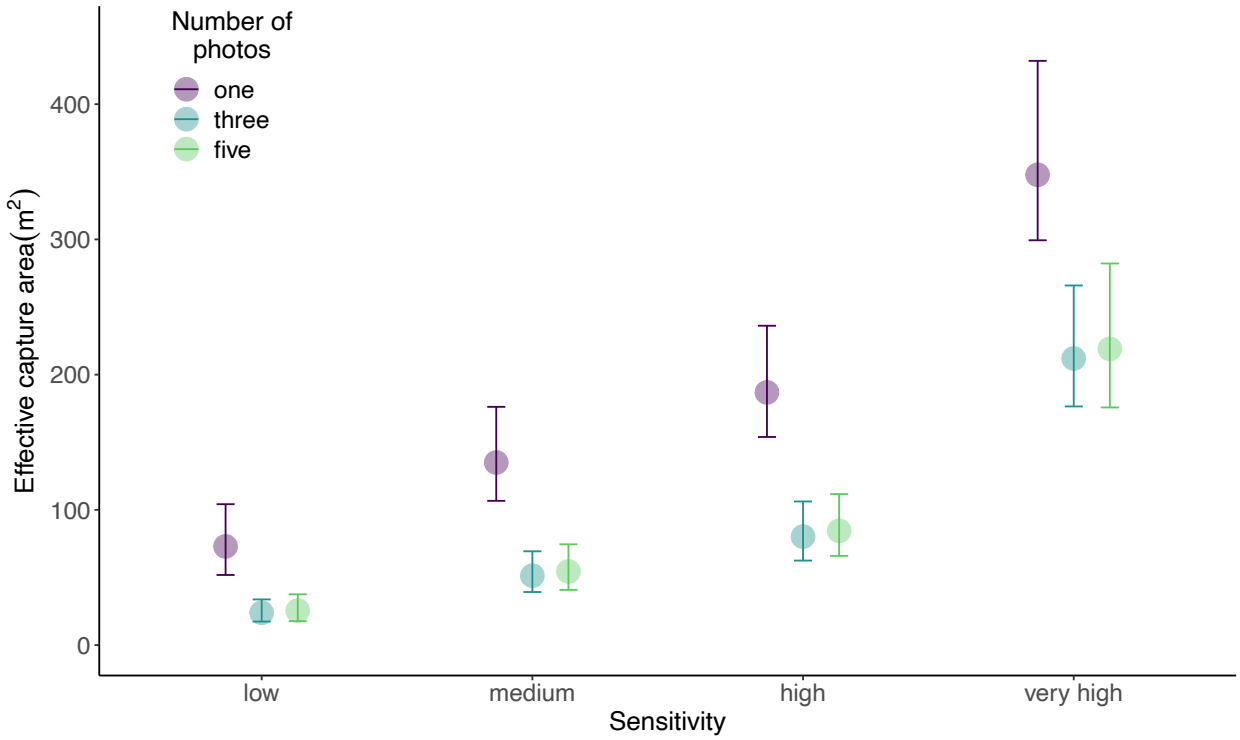

Figure 4. Effects of different sensitivity settings (low, medium, high, very high) and number of photos taken per each Passive Infrared Motion trigger (one, three, five) on the predicted Effective Capture Areas ($m^2 \pm$ SE) of Reconyx Hyperfire 2 camera traps (n = 26) predicted from Generalized Additive Mixed Models during our controlled setting trials for Case Study B.

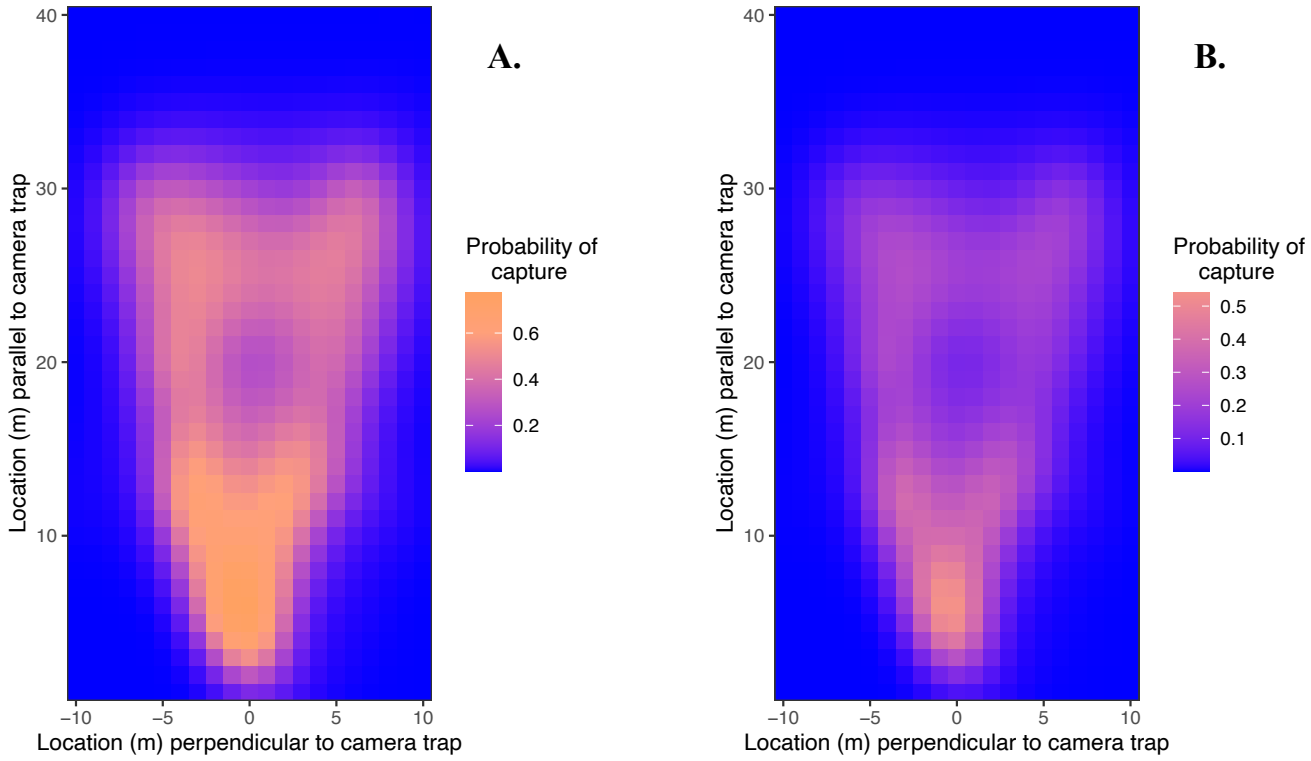

Figure 5. Predicted probabilities of photographic capture, predicted with Generalized Additive Mixed Models, on a 1x1 m grid for Reconyx Hyperfire 2 cameras, assuming a "medium" sensitivity setting, and a single photo taken for each Passive Infrared motion detector trigger during **A**. daytime trials and **B.** nighttime trials. Cameras are located at position [0,0] on each figure. The Adjusted Detection Areas (± SE) were determined to be 151 m^2 (122–191 m^2) for daytime (**A**) and 73 m^2 (53–101 m^2) for nighttime (**B**).

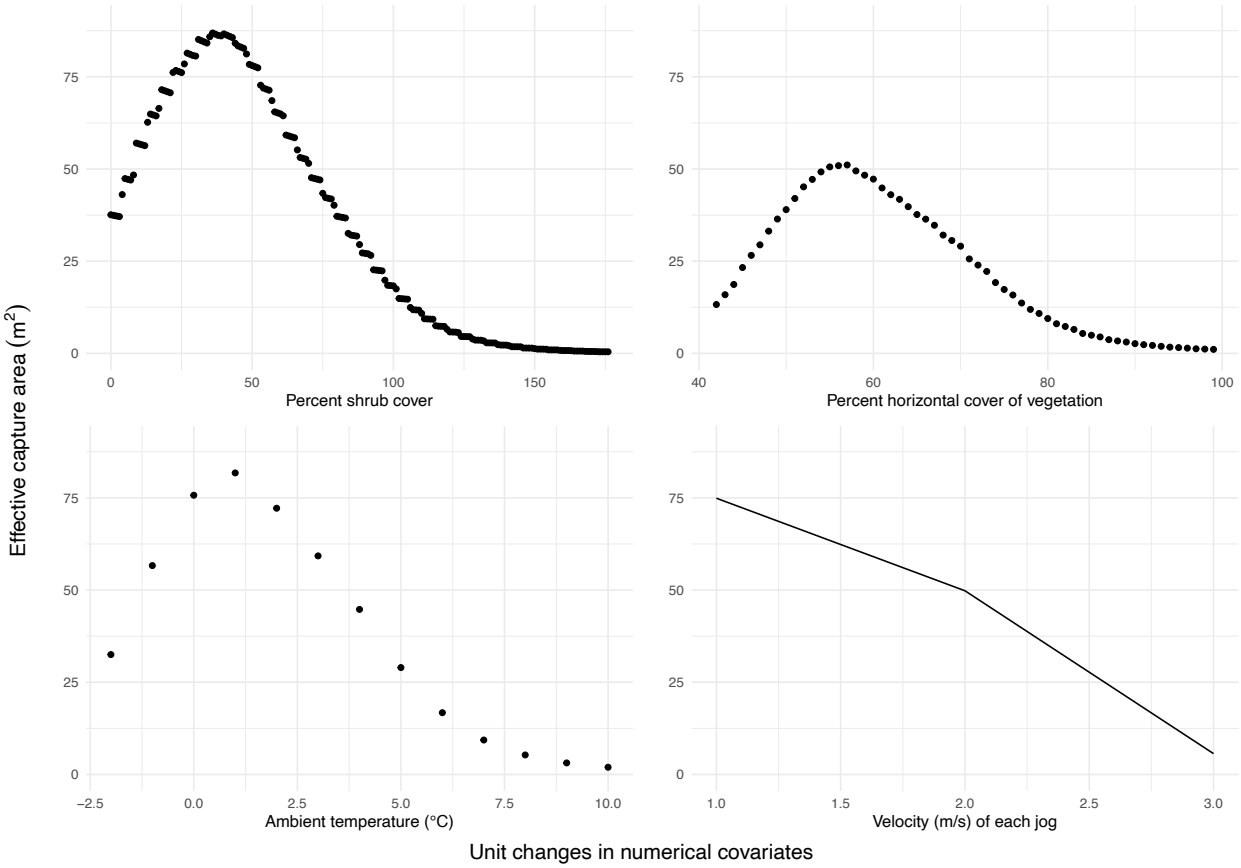

Figure 6. The predicted influence of unit changes of numerical covariates across their measured range in Case Study A, i.e., percent shrub cover, percent horizontal cover of vegetation, ambient air temperate (°C) at time of survey, and velocity (m/s) of each jog, on the Effective Capture Area at a given camera trap. For each numerical covariate of interest, all other covariates are held at their mean value for all predictions.